Journal of Power Sources 245 (2014) 953–957

Contents lists available at ScienceDirect

Journal of Power Sources

journal homepage: www.elsevier.com/locate/jpowsour

Short communication

Synthesis and characterization of $BaZr_{0.3}Ce_{0.5}Y_{0.2-x}Yb_xO_{3-\delta}$ proton conductor for solid oxide fuel cells

Zhen Shi [a], Wenping Sun [a], Wei Liu [a,b,*]

[a] CAS Key Laboratory of Materials for Energy Conversion, Department of Materials Science and Engineering, University of Science and Technology of China (USTC), Hefei 230026, PR China
[b] Key Laboratory of Materials Physics, Institute of Solid State Physics, Chinese Academy of Sciences, Hefei 230031, PR China

HIGHLIGHTS

- $BaZr_{0.3}Ce_{0.5}Y_{0.2-x}Yb_xO_{3-\delta}$ powders were synthesized via a combustion method.
- The phase structure and electrical conductivity of $BaZr_{0.3}Ce_{0.5}Y_{0.2-x}Yb_xO_{3-\delta}$ were investigated.
- $BaZr_{0.3}Ce_{0.5}Y_{0.2}O_{3-\delta}$ exhibits the highest conductivity.
- $BaZr_{0.3}Ce_{0.5}Y_{0.2}O_{3-\delta}$-based single cells achieved excellent performance at intermediate/low temperatures.

ARTICLE INFO

Article history:
Received 23 May 2013
Received in revised form
9 July 2013
Accepted 12 July 2013
Available online 20 July 2013

Keywords:
High temperature proton conductors
Electrical conductivity
Electrochemical performance
Solid oxide fuel cells

ABSTRACT

The acceptor-doped $BaCeO_3$–$BaZrO_3$ solid solution shows a good compromise between conductivity and chemical stability. Y and/or Yb doped $BaCeO_3$–$BaZrO_3$ solid solution $BaZr_{0.3}Ce_{0.5}Y_{0.2-x}Yb_xO_{3-\delta}$ (x = 0, 0.05, 0.1, 0.15, 0.2) powders are synthesized via a typical citrate–nitrate combustion method in this work. The crystal structure and electrical conductivity of $BaZr_{0.3}Ce_{0.5}Y_{0.2-x}Yb_xO_{3-\delta}$ are investigated. The XRD results reveal all the powders possess orthorhombic perovskite structure. The electrical conductivity decreases monotonously with increasing the proportion of Yb, and $BaZr_{0.3}Ce_{0.5}Y_{0.2}O_{3-\delta}$ exhibits the highest electrical conductivity. Single cells with $BaZr_{0.3}Ce_{0.5}Y_{0.2}O_{3-\delta}$ as the electrolyte are fabricated and tested, and the cell outputs excellent power density and stability. The peak power density of the cell reaches as high as 513 and 396 mW cm^{-2} at 650 and 600 °C, suggesting that $BaZr_{0.3}Ce_{0.5}Y_{0.2}O_{3-\delta}$-based fuel cells are promising solid oxide fuel cells (SOFCs) working at low temperatures.

1. Introduction

High temperature proton conductors (HTPCs) have great potential applications in SOFCs, gas sensors, and hydrogen separation membranes. Among all kinds of HTPCs, rare earth doped barium zirconate and barium cerate are the state-of-the-art materials [1–6]. The doped $BaCeO_3$ is considered as one of the best HTPCs for its high proton conductivity, but is unstable in CO_2 or H_2O containing atmospheres. In contrast, doped $BaZrO_3$ is quite stable, but it's difficult to prepare highly conductive $BaZrO_3$-based HTPCs due to its poor sintering activity.

A lot of work has been done to improve the chemical stability of $BaCeO_3$-based HTPCs and sintering activity of $BaZrO_3$-based HTPCs. Doped $BaCeO_3$–$BaZrO_3$ solid solutions were widely investigated and found to be good candidates for HTPCs because of their chemical stability and sufficient proton conductivity. The increase of Zr content in the solid solution can effectively promote the chemical stability, but is detrimental to the sintering activity and electrical conductivity [7,8]. Considering the stability and conductivity, $BaCe_{0.5}Zr_{0.3}Y_{0.2}O_{3-\delta}$ is a promising HTPC, which can achieve the compromise between chemical stability and conductivity [7,9], and has been employed as the electrolyte materials for SOFCs and solid oxide electrolysis cells [10–14].

The electrical conductivity of HTPCs is determined by the concentration and mobility of protons. As was reported, both the concentration and mobility of protons in $BaCeO_3$ and $BaZrO_3$-based HTPCs are closely related with the dopant. Y^{3+} (R^{VI} = 0.90 Å) and Yb^{3+} (R^{VI} = 0.868 Å) are considered to be favourable dopants in barium cerate and zirconate [15,16]. Recently, Y and Yb co-doped

* Corresponding author. CAS Key Laboratory of Materials for Energy Conversion, Department of Materials Science and Engineering, University of Science and Technology of China (USTC), Hefei 230026, PR China. Tel.: +86 0551 63606929; fax: +86 0551 63602586.
E-mail address: wliu@ustc.edu.cn (W. Liu).

0378-7753/$ – see front matter © 2013 Elsevier B.V. All rights reserved.
http://dx.doi.org/10.1016/j.jpowsour.2013.07.060

$BaZr_{0.1}Ce_{0.9}O_{3-\delta}$, $BaZr_{0.1}Ce_{0.7}Y_{0.1}Yb_{0.1}O_{3-\delta}$ (BZCYYb) [17], was reported to show the highest electrical conductivity among the serial composition $BaZr_{0.1}Ce_{0.7}Y_{0.2-x}Yb_xO_{3-\delta}$ in wet O_2. At the same time, BZCYYb also exhibits excellent sulphur and coking tolerance. Zhao et al. [18] studied Y and In co-doped $BaCeO_3$ and found that the electrical conductivity of $BaIn_{0.3-x}Y_xCe_{0.7}O_{3-\delta}$ increased with Y content. Imashuku et al. [19] investigated the effect of Sc and Y co-doping on the properties of $BaZr_{0.85}Sc_xY_{0.15-x}O_{3-\delta}$. Sc could enhance the sintering and hence the grain-boundary conductivity, and $BaZr_{0.85}Sc_{0.05}Y_{0.13-\delta}$ exhibited the highest conductivity. Ito et al. [20] reported that the electrical conductivity was significantly reduced after introducing In or Ga into $BaZr_{0.9}Y_{0.1}O_{3-\delta}$, although the sintering activity was significantly improved. To sum up, it can be inferred that the co-doping strategy has various effects on the properties of doped $BaCeO_3$ and $BaZrO_3$-based HTPCs. For the proton-conducting doped-ceria oxides, Fang and Yan found that La and Ca or Sm co-doping enhanced the proton conductivity of La doped CeO_2 [21,22].

In this work, the influence of Y and Yb co-doping on the properties of $BaCe_{0.5}Zr_{0.3}Y_{0.2-x}Yb_xO_{3-\delta}$ proton conductors was investigated. $BaCe_{0.5}Zr_{0.3}Y_{0.2-x}Yb_xO_{3-\delta}$ powders were synthesized via a typical combustion method. Single cells based on $BaCe_{0.5}Zr_{0.3}Y_{0.2}O_{3-\delta}$, which showed the highest conductivity, were fabricated and evaluated.

2. Experimental

2.1. Powder synthesis and pellet fabrication

$BaZr_{0.3}Ce_{0.5}Y_{0.2-x}Yb_xO_{3-\delta}$ (x = 0, 0.05, 0.1, 0.15, 0.2) powders were synthesized via a citric acid–nitrate gel combustion process [23]. The as-prepared powders were calcined at 1050 °C in the air for 3 h to form a single phase. The $BaZr_{0.3}Ce_{0.5}Y_{0.2-x}Yb_xO_{3-\delta}$ powders were grinded with a mortar and pestle before preparing green pellet samples. The $BaZr_{0.3}Ce_{0.5}Y_{0.2-x}Yb_xO_{3-\delta}$ pellets were fabricated by an uni-axial pressing method with a pressure of 200 MPa. Afterwards, the pellets were sintered at 1550 °C for 10 h in air to obtain pellet samples for conductivity measurement.

2.2. Characterization

Phase analysis was examined by an X-ray diffractometer (XRD; Rigaku TTR-III) with CuKα radiation (λ = 1.54 Å). Scanning electron microscope (SEM; JEOL JSM-6700F) was employed to study the microstructure of the sintered pellets. Pt paste was painted on both sides of each pellet followed by firing at 950 °C for 1 h, getting porous electrodes. Ag wire was used as the lead wire. The total resistance of $BaZr_{0.3}Ce_{0.5}Y_{0.2-x}Yb_xO_{3-\delta}$ pellets in humidified hydrogen (2% H_2O) was determined according to the electrochemical impedance spectroscopy (EIS) which was performed by an impedance analyzer (CHI604B, Chenhua, Shanghai) in the temperature range of 350–800 °C. A 5 mA A.C. signal was applied and the sweeping frequency ranged from 100 kHz to 0.1 Hz. The flowing rate of wet hydrogen was around 50 mL min^{-1}.

2.3. Single cell fabrication and test

The anode supported half cells with a tri-layered structure were fabricated by a typical dry-pressing method then co-fired at 1400 °C for 5 h [5]. The NiO–$BaZr_{0.1}Ce_{0.7}Y_{0.2}O_{3-\delta}$ composite powders prepared by a one-step combustion process was utilized to fabricate the anode functional layer between the NiO–$BaZr_{0.1}Ce_{0.7}Y_{0.2}O_{3-\delta}$ (65:35, weight ratio, 20 wt% starch was added as pore former) anode support and $BaZr_{0.3}Ce_{0.5}Y_{0.2}O_{3-\delta}$ electrolyte film. The $Sm_{0.5}Sr_{0.5}CoO_{3-\delta}$–$Ce_{0.8}Sm_{0.2}O_{2-\delta}$ (SSC–SDC) composite cathode was brush-painted onto the electrolyte film followed by firing at 950 °C for 2 h, obtaining the porous cathode layer with an area of 0.237 cm^2. The single cell was tested with a home-made cell testing system at temperatures from 400 to 650 °C with humidified hydrogen (~2% H_2O, 30 mL min^{-1}) as the fuel gas and static air as the oxidant. The I–V curves of the cell were measured with a DC Electronic Load (ITech Electronics model IT8511), and the electrochemical impedance spectra of the cell under open circuit conditions were performed by an impedance analyzer (CHI604B, Chenhua, Shanghai).

3. Results and discussion

3.1. Phase structure

Fig. 1 is the XRD patterns of the $BaZr_{0.3}Ce_{0.5}Y_{0.2-x}Yb_xO_{3-\delta}$ powders prepared by the combustion method after calcined at 1050 °C for 3 h in air. All the diffraction peaks in the patterns correspond to the orthorhombic perovskite structure, which also indicates that all the powders possess the same crystal structure. As was reported, the phase structure of $BaCeO_3$–$BaZrO_3$ solid solution is highly dependent on the concentration of Zr [7,8,24,25]. Katahira et al. [8] claimed an orthorhombic structure in $BaCe_{0.9-x}Zr_xY_{0.1}O_{3-\delta}$ for x = 0.1 and 0.2 while cubic for $x \geq 0.3$. Fabbri et al. [7] and Guo et al. [24] reported that the phase structure of $BaCe_{0.8-x}Zr_xY_{0.2}O_{3-\delta}$ is orthorhombic when x = 0.1–0.5 and cubic when x = 0.6–0.8. Since the ion radius of Y^{3+} (R^{VI} = 0.90 Å) and Yb^{3+} (R^{VI} = 0.868 Å) is close to each other and the doping concentration variation of Y or Yb is very limited, no clear peak shift to the higher angle can be observed in the XRD patterns. In Yang's report about $BaZr_{0.1}Ce_{0.7}Y_{0.2-x}Yb_xO_{3-\delta}$, there was also no obvious peak shift in the XRD patterns of the powders [17]. The cell parameters, cell volumes, as well as tolerance factors (t) of $BaZr_{0.3}Ce_{0.5}Y_{0.2-x}Yb_xO_{3-\delta}$ powders are calculated, as given in Table 1. One can see that there is only a slight shrinkage of the cell volume with increasing the content of Yb. The variation of cell parameters reveals that Y is substantially substituted by Yb.

3.2. Electrical conductivity

Shown in Fig. 2 are the SEM images of the cross-sectional morphology of the $BaZr_{0.3}Ce_{0.5}Y_{0.2-x}Yb_xO_{3-\delta}$ pellets sintered at 1550 °C for 10 h. As can be seen, all the samples have similar microstructures, suggesting that the sintering activity is not affected

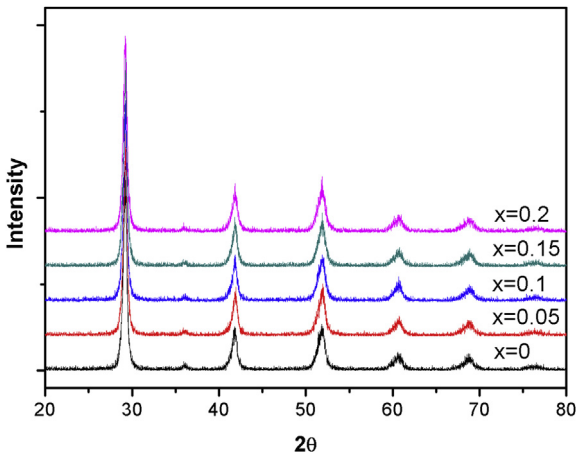

Fig. 1. XRD patterns of $BaZr_{0.3}Ce_{0.5}Y_{0.2-x}Yb_xO_{3-\delta}$ ($0 \leq x \leq 0.2$) powders prepared via combustion method and calcined at 1050 °C for 3 h.

Table 1
Summary of crystal parameters and tolerance factors of as-synthesized $BaZr_{0.3}Ce_{0.5}Y_{0.2-x}Yb_xO_{3-\delta}$ powders.

x	Crystal symmetry	a/Å	b/Å	c/Å	Cell vol/Å^3	t
0	Orthorhombic	6.1329	6.1318	8.6372	324.81	0.9633
0.05	Orthorhombic	6.1140	6.1089	8.6633	323.57	0.9640
0.10	Orthorhombic	6.1033	6.0992	8.6736	322.88	0.9648
0.15	Orthorhombic	6.1084	6.0965	8.5929	320.00	0.9655
0.20	Orthorhombic	6.1042	6.0932	8.5906	319.52	0.9662

after substituting Y with Yb in the oxides. The microstructure similarity makes it possible to study the electrical conductivity of the oxides comparatively. Fig. 3(a) shows the Arrhenius plots of the total electrical conductivity of $BaZr_{0.3}Ce_{0.5}Y_{0.2-x}Yb_xO_{3-\delta}$ pellets in wet hydrogen at temperatures from 650 to 800 °C. As can be found, the conductivity decreases with increasing the proportion of Yb in the oxides, especially at the high-temperature region (650–800 °C). At 700 °C, the conductivity is 1.0×10^{-2}, 0.94×10^{-2}, 0.85×10^{-2}, 0.7×10^{-2}, and 0.67×10^{-2} S cm^{-1} for $BaZr_{0.3}Ce_{0.5}Y_{0.2-x}Yb_xO_{3-\delta}$ with $x = 0$, 0.05, 0.1, 0.15 and 0.2, respectively. At high temperatures, protons in pervoskite-type proton conductors are generally believed to transport in the following steps: 1) a proton associate with a fixed oxygen atom; 2) the proton-oxygen bond reorientates under the influence of the neighbour oxygen atom; 3) the proton starts to oscillate between the two oxygen atoms and eventually moves to the neighbour oxygen [1,26]. According to the experimental and simulation results, the binding energy between $OH^{\bullet}$ and M_B' varied with the dopant. In Islam's results, the binding energies of $OH^{\bullet}$–M_B' hydroxyl–dopant pairs at the nearest-neighbour sites were simulated to be −0.26, −0.35 and −0.58 eV for Y, Yb and In, respectively, which were also in good agreement with the experiment results [15,27]. A more negative value of the binding energy represents a more stable state for the hydroxyl–dopant pairs, indicating that the associated proton is more difficult to move around. In other words, the proton mobility is closely related to the binding energies of $OH^{\bullet}$–M_B'. Notably, this hypothesis is well verified by the electrical conductivity variation of $BaZr_{0.3}Ce_{0.5}Y_{0.2-x}Yb_xO_{3-\delta}$ in this work. Due to the higher binding energies of $OH^{\bullet}$–Yb_{Ce}', the electrical conductivity of $BaZr_{0.3}Ce_{0.5}Y_{0.2-x}Yb_xO_{3-\delta}$ decreased significantly with increasing Yb in the high-temperature region. When the temperature is further reduced (below 600 °C), the electrical conductivity tends to be comparable (Fig. 3(b)). An inflection point of the σ–T plots

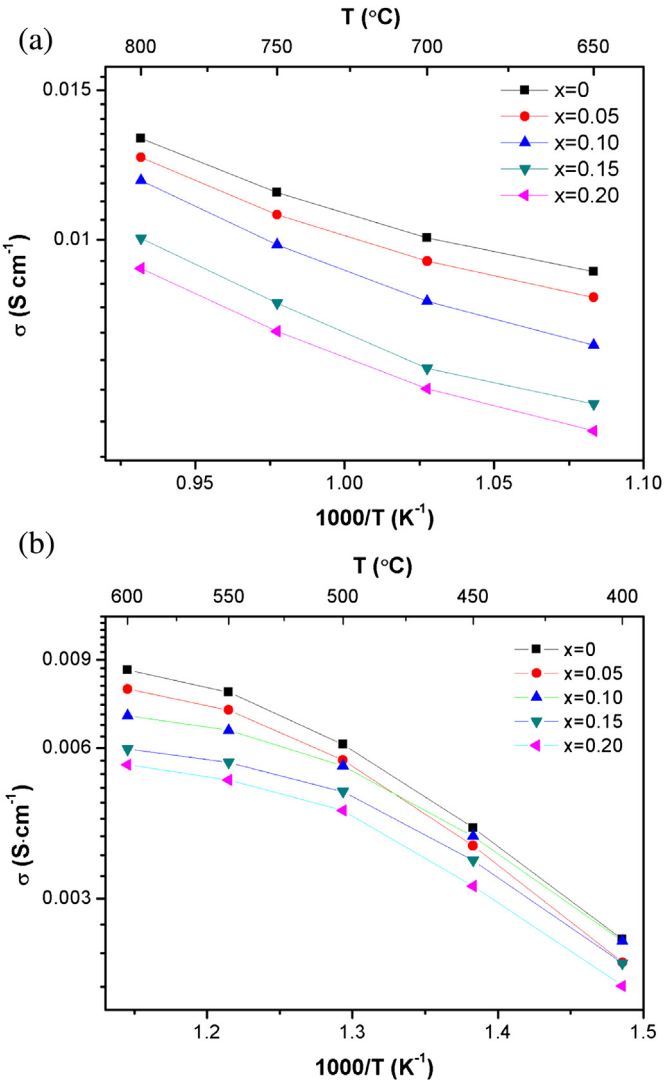

Fig. 3. Arrhenius plots of the total electrical conductivity (σ) of $BaZr_{0.3}Ce_{0.5}Y_{0.2-x}Yb_xO_{3-\delta}$ pellets in wet hydrogen (~2% H_2O) at temperatures: 800 to 650 °C (a), 600 to 400 °C (b).

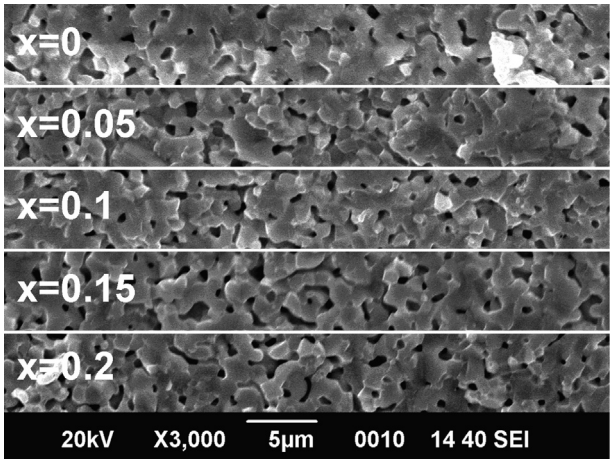

Fig. 2. Merged SEM images of the cross-sectional morphology of $BaZr_{0.3}Ce_{0.5}Y_{0.2-x}Yb_xO_{3-\delta}$ ($0 \le x \le 0.2$) pellets sintered at 1550 °C for 10 h.

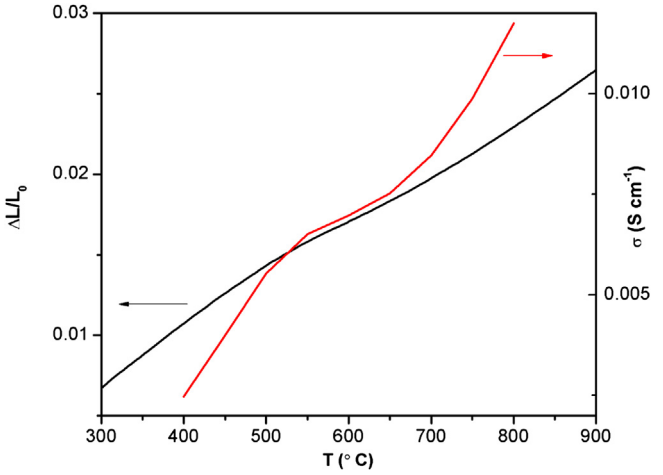

Fig. 4. Thermal expansion plots and Arrhenius plots of the total electrical conductivity of $BaZr_{0.3}Ce_{0.5}Y_{0.1}Yb_{0.1}O_{3-\delta}$ pellet at temperatures from 400 to 800 °C.

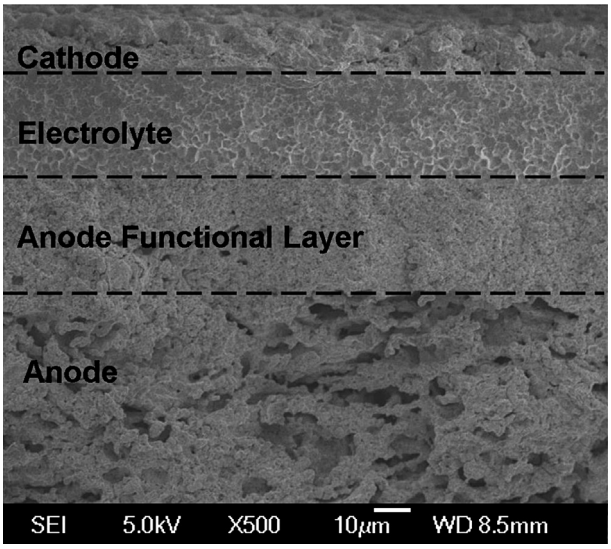

Fig. 5. SEM image of cross-sectional morphology of tested single cell based on $BaZr_{0.3}Ce_{0.5}Y_{0.2}O_{3-\delta}$.

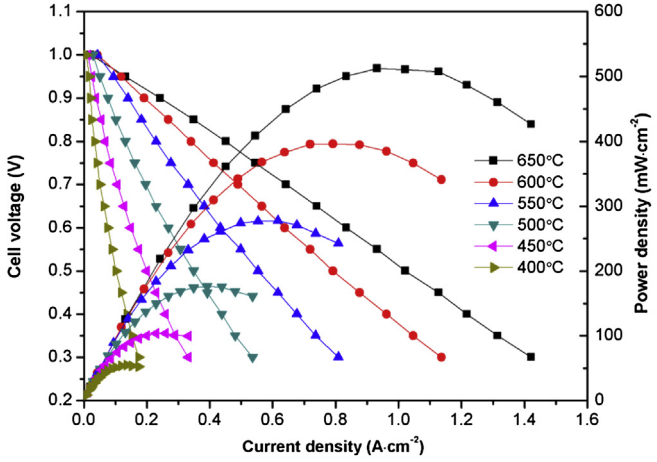

Fig. 6. *I–V* and power density curves of the $BaZr_{0.3}Ce_{0.5}Y_{0.2}O_{3-\delta}$-based single cell at different operating temperatures with wet hydrogen (2% H_2O) as the fuel and static air as the oxidant.

around 600 °C can be observed, which might result from the phase transformation from cubic to orthorhombic of the oxides [28], as can be also seen in Fig. 4. Accompanying the structure distortion, the symmetry of the oxides is significantly reduced, which would be detrimental to proton mobility. Compared to the cubic cell, the orthorhombic cell with a larger cell parameter and anisotropy has less paths for proton migration due to the symmetry reduction [29]. In this case, the dopants would not affect the proton mobility too much, and hence would not influence the conductivity significantly.

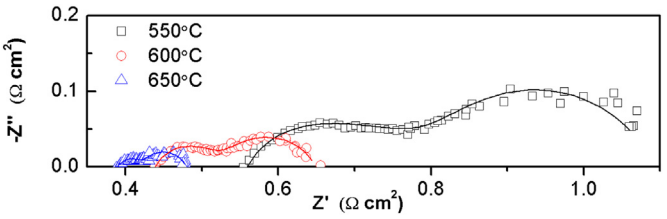

Fig. 7. Electrochemical impedance spectra of the single cell measured under open circuit conditions.

3.3. Single cell performance

$BaZr_{0.3}Ce_{0.5}Y_{0.2}O_{3-\delta}$ was further evaluated as the electrolyte material due to its highest conductivity among the series. Fig. 5 shows the SEM image of the cross-sectional morphology of the tested cell. It can be seen that the $BaZr_{0.3}Ce_{0.5}Y_{0.2}O_{3-\delta}$ electrolyte film is about 27 μm in thickness. The electrolyte film is fully dense, free from crack and bonds firmly to the electrode layers. The excellent microstructure is beneficial for obtaining single cells with low resistances, thus outputting high power performance. The open circuit voltages (OCVs) of the cell were 1.01, 1.02, 1.03, 1.05, 1.06 and 1.07 V at 650, 600, 550, 500, 450 and 400 °C, respectively, further confirming the high density of the electrolyte film. The *I–V* and power density curves of the cell is presented in Fig. 6. One can see that the cell exhibits excellent power performance. The peak power density achieved 513, 396, 278, 176, 104 and 54 mW cm^{-2} at 650, 600, 550, 500, 450 and 400 °C, respectively. At the output voltage of 0.7 V, the power densities still reached 450, 340, 232, 137, 74 and 36 mW cm^{-2}, respectively. The cell performance is largely improved as compared to those $BaZr_{0.3}Ce_{0.5}Y_{0.2}O_{3-\delta}$-based cells, as shown in Table 2 [12–14,30]. Ding et al. [13] reported a 20-μm-thick $BaZr_{0.3}Ce_{0.5}Y_{0.16}Zn_{0.04}O_{3-\delta}$-based single cell and the peak power densities were 364 and 246 mW cm^{-2} at 650 and 600 °C, respectively. Furthermore, the cell performance is even comparable with those ever-reported best performances of $BaZr_{0.1}Ce_{0.7}Y_{0.2}O_{3-\delta}$-based cells, with peak power densities of 598 and 504 mW cm^{-2} at 650 °C reported by Yang et al. [31] and Sun et al. [32], respectively.

To further illustrate the good performance of the single cell, electrochemical impedance spectra (EIS) of the cell were measured and discussed. Fig. 7 shows the EIS of the cell measured under open circuit conditions from 650 to 550 °C. The ohmic resistances (R_{ohm}), which are determined by the electrolyte resistance, are 0.385, 0.436 and 0.646 Ω cm^2 at 650, 600 and 550 °C, respectively; while the polarization resistances (R_p) are 0.09, 0.2 and 0.57 Ω cm^2, which are mainly associated with the electrode materials and microstructures. As compared with the previous results, both R_{ohm} and R_p values are lower than other $BaZr_{0.3}Ce_{0.5}Y_{0.2}O_{3-\delta}$-based cells and many $BaZr_{0.1}Ce_{0.7}Y_{0.2}O_{3-\delta}$-based cells. The excellent performance of the present cell is definitely induced by the low cell resistances. The low R_{ohm} values should be attributed to the highly dense and thin electrolyte film, and the highly active cathode materials and

Table 2
Summary of the electrolyte film thickness (μm), cathode material and peak power density (PPD/mW cm^{-2}) of the cells with $BaZr_{0.3}Ce_{0.5}Y_{0.2}O_{3-\delta}$-like electrolytes reported in literature.

Electrolyte	Thickness	Cathode	PPD	Reference
$BaZr_{0.3}Ce_{0.5}Y_{0.16}Zn_{0.04}O_{3-\delta}$	30	$Ba_{0.5}Sr_{0.5}Zn_{0.2}Fe_{0.8}O_{3-\delta}$	236 (700 °C)	[12]
$BaZr_{0.3}Ce_{0.5}Y_{0.16}Zn_{0.04}O_{3-\delta}$	20	$Sm_{0.5}Sr_{0.5}CoO_{3-\delta}$–BZCYZ	364 (650 °C)	[13]
$BaZr_{0.3}Ce_{0.5}Y_{0.16}Zn_{0.04}O_{3-\delta}$	25	$LaSr_3Co_{1.5}Fe_{1.5}O$–BZCYZ	250 (650 °C)	[14]
$BaZr_{0.3}Ce_{0.5}Y_{0.16}Zn_{0.04}O_{3-\delta}$	20	$PrBaCo_2O_{5+\delta}$–BZCYZ	266 (650 °C)	[30]
$BaZr_{0.3}Ce_{0.5}Y_{0.2}O_{3-\delta}$	27	$Sm_{0.5}Sr_{0.5}CoO_{3-\delta}$–SDC	513 (650 °C)	This work

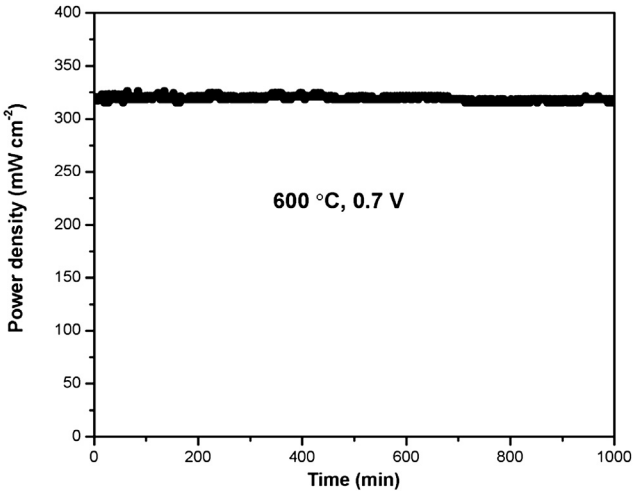

Fig. 8. Short-term performance stability of single cell tested at 600 °C at an output voltage of 0.7 V.

fine electrode microstructures should be responsible for the low R_p values.

Moreover, the short-term stability of the cell performance was also tested at 600 °C with a constant output voltage of 0.7 V, and the dependence of power density on the elapsed time is displayed in Fig. 8. The power density of around 320 mW cm^{-2} was observed to keep constant without degradation during the operation. The stable performance indicates that the $BaZr_{0.3}Ce_{0.5}Y_{0.2}O_{3-\delta}$ is chemically stable under fuel cell conditions and is a good candidate proton-conducting electrolyte material for SOFCs. Moreover, the high performance combining with the good stability demonstrates that the $BaZr_{0.3}Ce_{0.5}Y_{0.2}O_{3-\delta}$-based cell is a promising SOFC applicable at reduced temperatures.

4. Conclusions

In this work, the dopant effect on the electrical conductivity of $BaZr_{0.3}Ce_{0.5}Y_{0.2-x}Yb_xO_{3-\delta}$ ($x = 0$, 0.05, 0.1, 0.15, 0.2) was carefully studied. To achieve high proton conductivity, Y was found to be a better dopant than Yb. The conductivity of $BaZr_{0.3}Ce_{0.5}Y_{0.2-x}Yb_xO_{3-\delta}$ decreased with increasing Yb in wet hydrogen, and $BaZr_{0.3}Ce_{0.5}Y_{0.2}O_{3-\delta}$ exhibited the highest proton conductivity among the series. Moreover, $BaZr_{0.3}Ce_{0.5}Y_{0.2}O_{3-\delta}$-based single cells outputted excellent power density and stability. The present results demonstrate that $BaZr_{0.3}Ce_{0.5}Y_{0.2}O_{3-\delta}$ is a promising stable proton-conducting electrolyte material for SOFCs.

Acknowledgements

This work was financially supported by the Natural Science Foundation of China (Grant No. 21076204) and the Ministry of Science and Technology of China (Grant No. 2012CB215403).

References

[1] H. Iwahara, Solid State Ionics 86–88 (1996) 9–15.
[2] H. Iwahara, Solid State Ionics 125 (1999) 271–278.
[3] W. Sun, M. Liu, W. Liu, Advanced Energy Materials (2013).
[4] W. Sun, Z. Zhu, Z. Shi, W. Liu, Journal of Power Sources 229 (2013) 95–101.
[5] W. Sun, L. Yan, Z. Shi, Z. Zhu, W. Liu, Journal of Power Sources 195 (2010) 4727–4730.
[6] C. Zuo, S. Zha, M. Liu, M. Hatano, M. Uchiyama, Advanced Materials 18 (2006) 3318–3320.
[7] E. Fabbri, A. D'Epifanio, E. Di Bartolomeo, S. Licoccia, E. Traversa, Solid State Ionics 179 (2008) 558–564.
[8] K. Katahira, Y. Kohchi, T. Shimura, H. Iwahara, Solid State Ionics 138 (2000) 91–98.
[9] C.D. Zuo, S.E. Dorris, U. Balachandran, M.L. Liu, Chemistry of Materials 18 (2006) 4647–4650.
[10] Y.Y. Rao, S.H. Zhong, F. He, Z.B. Wang, R.R. Peng, Y.L. Lu, International Journal of Hydrogen Energy 37 (2012) 12522–12527.
[11] F. He, D. Song, R. Peng, G. Meng, S. Yang, Journal of Power Sources 195 (2010) 3359–3364.
[12] B. Lin, M.J. Hu, J.J. Ma, Y.Z. Jiang, S.W. Tao, G.Y. Meng, Journal of Power Sources 183 (2008) 479–484.
[13] H.P. Ding, X.J. Xue, X.Q. Liu, G.Y. Meng, Journal of Alloys and Compounds 494 (2010) 233–235.
[14] S. Zhang, L. Bi, L. Zhang, Z. Tao, W. Sun, H. Wang, W. Liu, Journal of Power Sources 188 (2009) 343–346.
[15] M.S. Islam, P.R. Slater, J.R. Tolchard, T. Dinges, Dalton Transactions (2004) 3061–3066.
[16] H. Iwahara, T. Yajima, H. Ushida, Solid State Ionics 70 (1994) 267–271.
[17] L. Yang, S. Wang, K. Blinn, M. Liu, Z. Liu, Z. Cheng, M. Liu, Science 326 (2009) 126–129.
[18] F. Zhao, Q. Liu, S. Wang, K. Brinkman, F. Chen, International Journal of Hydrogen Energy 35 (2010) 4258–4263.
[19] S. Imashuku, T. Uda, Y. Nose, K. Kishida, S. Harada, H. Inui, Y. Awakura, Journal of The Electrochemical Society 155 (2008) B581–B586.
[20] N. Ito, H. Matsumoto, Y. Kawasaki, S. Okada, T. Ishihara, Solid State Ionics 179 (2008) 324–329.
[21] L.T. Yan, W.P. Sun, L. Bi, S.M. Fang, Z.T. Tao, W. Liu, International Journal of Hydrogen Energy 35 (2010) 4508–4511.
[22] S.M. Fang, L. Bi, L.T. Yan, W.P. Sun, C.S. Chen, W. Liu, Journal of Physical Chemistry C 114 (2010) 10986–10991.
[23] Z. Zhu, L. Yan, W. Sun, H. Liu, T. Liu, W. Liu, Journal of Power Sources 217 (2012) 431–436.
[24] Y. Guo, Y. Lin, R. Ran, Z. Shao, Journal of Power Sources 193 (2009) 400–407.
[25] K.H. Ryu, S.M. Haile, Solid State Ionics 125 (1999) 355–367.
[26] K.D. Kreuer, A. Fuchs, J. Maier, Solid State Ionics 77 (1995) 157–162.
[27] J. Lv, L. Wang, D. Lei, H. Guo, R.V. Kumar, Journal of Alloys and Compounds 467 (2009) 376–382.
[28] K.S. Knight, Solid State Ionics 145 (2001) 275–294.
[29] K.D. Kreuer, Solid State Ionics 125 (1999) 285–302.
[30] M.F. Jin, X.L. Zhang, Y. Qiu, J.M. Sheng, Journal of Alloys and Compounds 494 (2010) 359–361.
[31] L. Yang, C. Zuo, S. Wang, Z. Cheng, M. Liu, Advanced Materials 20 (2008) 3280–3283.
[32] W.P. Sun, L.T. Yan, B. Lin, S.Q. Zhang, W. Liu, Journal of Power Sources 195 (2010) 3155–3158.